Journal of Engineering Mathematics **36:** 255–275, 1999.

Capillary instability and breakup of a viscous thread

C. POZRIKIDIS
University of California, San Diego; La Jolla, California 92093-0411, USA; e-mail: cpozrikidis@ucsd.edu

Received 5 August 1998; accepted in revised form 12 January 1999

Abstract. Papageorgiou derived a similarity solution that describes the asymptotic behavior of a thinning viscous thread suspended in vacuum, near the critical time and around the location of breakup. The motion is driven by surface tension, and the fluid inertia is neglected throughout the evolution. To assess the physical relevance of the similarity solution, the evolution of an infinite thread immersed in an ambient fluid with arbitrary viscosity, subject to periodic axisymmetrtic perturbations is simulated through solution of the equations of Stokes flow by a boundary integral method. The results show that when the thread is suspended in vacuum, the similarity solution accurately describes the process of thinning over an extended length of the thread between the developing bulges, and captures the late stages of breakup for a broad range of initial conditions. But a small amount of ambient fluid viscosity, as small as 0·05 times the viscosity of the thread fluid, drastically alters the nature of the motion by shifting the location of the breakup points toward the bases of developing bulges, and causing the thread to develop locally asymmetric shapes.

Key words: viscous flow, hydrodynamic instability, similarity solutions, boundary integral methods.

1. Introduction

The mixing of two immiscible fluids generally proceeds in two stages. The first stage involves the formation of sheet-like or thread-like interfacial structures whose size is small compared to the dimensions of the enclosing container or apparatus; this is typically accomplished by mechanical agitation in static and dynamic mixing devices, sheet formation at slits, or jet formation at nozzles and slots. The second stage involves the disintegration of these structure due to a rapidly varying ambient motion in a turbulent flow, or to the development of instabilities associated with viscosity contrast or surface tension. Accordingly, given the physical properties of the fluids, the smallest size of the dispersed phase is determined by the shortest length scale of the active fluid motion, which may be identified with the Kolmogorov scale of a turbulent flow, or set inversely proportional to a power of the capillary number expressing the relative importance of viscous stresses and capillary pressure due to surface tension.

For example, in industrial mixing devices, emulsions are typically produced by agitating two fluids to generate thread-like structures, and then relying on small-scale fluctuations or surface-tension to break the threads into small drops (*e.g.* Tjahjadi and Ottino [1]). A further increase in the rate of agitation causes the elongation and breakup of the dispersed drops into smaller fragments, but this only occurs when the rate-of-deformation of the ambient flow is sufficiently high, or the viscosity of the dispersed phase is comparable to, or less than, the viscosity of the ambient fluid; highly viscous drops in a simple shear flow cannot be made to elongate beyond a threshold even in the absence of surface tension. Establishing the relation between the macroscopic variables of a mixing process and the dynamics of the microstructure defines an important area of study within the general context of two-phase flow.

There are several further applications where the breakup of a liquid thread due to surface tension plays an important role, or receives special attention in achieving a desired goal. For example, in liquid-liquid extraction processes in perforated plate columns, jets of the dispersed phase are formed at each perforation at sufficiently high flow rates, only to break up at a certain distance away from the plate (Skelland and Walker [2], Skelland and Slaymaker [3]). Other applications include the breakup of liquid jets emanating from ink-jet nozzles in printing technology (*e.g.* Bogy [4], Allen *et al.* [5]), spraying and atomization, and the pinch-off of pendant drops (Henderson *et al.* [6]). Examples from the field of life sciences include the instability and breakup of the threads comprising a spider's web (Boys [7]).

The instability of a liquid thread has been the object of a large number of theoretical and experimental investigations, as reviewed by Eggers [8] and Lin and Reitz [9]. Plateau [10] and Rayleigh [11, 12] first established that a circular inviscid jet, or circular liquid thread, both suspended in vacuum, break up due to surface tension to yield a sequence of drops. For sinusoidal perturbations with wave number k, the thread or jet is unstable when $ka < 1$, where a is the unperturbed thread radius. That is, the thread or jet is unstable when the wave length of a perturbation, $L = 2\pi/k$, is larger than the thread circumferencial arc length.

Weber [13] and Tomotika [14] extended Rayleigh's analysis taking into consideration the effect of the viscosity of the ambient fluid. Their results showed that the instability criterion $ka < 1$ remains unchanged irrespective of the physical properties of the thread and ambient fluid. In fact, Goren [15, 16] showed the criterion remains valid even in the presence of one or two coaxial cylindrical surfaces confining an annular layer (see also Newhouse and Pozrikidis [17]). Further theoretical studies investigated the growth of spatially developing perturbations and the evolution of non-axisymmetric perturbations [4], while laboratory observations confirmed the ability of the linear stability theory to predict the initial growth of small-amplitude perturbations (*e.g.* Rumscheidt and Mason [18], Elemans *et al.* [19], Janssen [20]). In an effort to extend the predictive power of the linear theory, several authors carried out perturbation expansions with respect to the ratio of the amplitude and wave length of the perturbation, as reviewed by Bogy [4] and Eggers [8], or built asymptotic expansions based on the long wavelength or slender-thread approximation, as reviewed by Papageorgiou [21]. Weber [13] and Lee [22] led these efforts by developing one-dimensional models to describe the evolution of long waves.

Because of its importance in jet or thread disintegration, the local dynamics of a thinning thread close to the time and near the location of breakup has received special attention. Renardy [23] considered the evolution of a thread suspended in vacuum undergoing instability under conditions of Stokes flow, and showed that the thin-thread equations admit singular solutions according to which the radius of thread tends to zero at a finite time. Eggers [24] and Papageorgiou [25] discovered similarity solutions of the thin-thread equations, respectively, for Navier-Stokes and Stokes flow; both were generalized by Renardy [26] and Brenner *et al.* [27]. The similarity solutions confirm that the thread breaks up at a finite time, albeit following different functional forms. The Stokes flow solution predicts that the shape of the interface and velocity field are symmetric about the point of breakup, whereas the Navier-Stokes solution predicts unsymmetric flows and shapes. Numerical solutions by Eggers and Papageorgiou confirmed the relevance of the similarity solutions for a broad range of initial conditions, in the context of thin-thread asymptotics.

Numerical simulations of the Rayleigh instability, outside the linear and weakly nonlinear regimes or for finite-amplitude perturbations, were performed on several occasions. Bousfield *et al.* [28] simulated the instability of Newtonian and non-Newtonian threads at zero and

nonzero Reynolds numbers using a finite element method. Mansour and Lundgren [29] simulated the instability of an inviscid jet using a boundary-integral method for potential flow. Tjahjadi, Stone and Ottino [30], and Newhouse and Pozrikidis [17] simulated the evolution of elongated drops, threads, and annular layers at vanishing Reynolds number using boundary-integral methods. Janssen [20] performed further simulations using a finite-element method. The numerical results of Newhouse and Pozrikidis [17] established the importance of the ratio of viscosity of the thread to that of the ambient fluid on the location of the point of breakup and on the size of the emerging primary and satellite drops. More recently, Richards *et al.* [31, 32] used the volume-of-fluid method to simulate the capillary breakup of a jet that is injected into another fluid at non-zero Reynolds numbers, under a broad range of conditions. A detailed numerical investigation of the local dynamics near the critical time and around the location of break up, however, has not been presented.

Lister and Stone [33] discussed the nature of capillary breakup of a viscous thread surrounded by another viscous fluid. Using scaling arguments, they showed that the viscosity of the ambient fluid, however small, becomes important sufficiently close to the time of breakup. Moreover, Lister and Stone simulated with high-accuracy numerics the relaxation of an extended axisymmetric drop whose viscosity is equal to that of the ambient fluid, and obtained numerical evidence that a self-similar behavior is established near pinching. On either side of the point of pinching, the interface develops conical shapes with different cone angles, in agreement with the earlier simulations of Newhouse and Pozrikidis [17]. An interesting new feature is that the axial velocity near the region of minimum thread radius appears to increase at a logarithmic rate, apparently due to the asymmetry of the conical shapes.

The main objective of the present study is to assess the physical relevance of the similarity solution of the thin-thread equations for Stokes flow developed by Papageorgiou [25]. For this purpose, we use the boundary-integral method to simulate the evolution of an infinite viscous thread subject to axisymmetric perturbations, with emphasis on the behavior near the point of breakup. The results will confirm that the similarity solution arises from a broad range of initial conditions, and will reveal that a small amount of ambient fluid viscosity alters the character of the motion in a profound way.

2. Local dynamics near breakup

As a prelude to the numerical investigation, we review the equations of thin-thread evolution and the Papageorgiou similarity solution, recasting them into our notation. Consider the region near the minimum radius of a thinning axisymmetric thread immersed in an inviscid ambient fluid, with the interface exhibiting constant surface tension γ, as depicted in Figure 1(a). In polar cylindrical coordinates (x, σ, φ), the radius of the thread is described by the equation

$$\sigma = f(x, t). \tag{2.1}$$

The motion is subject to the conditions that

(a) the shear stress vanishes at the interface,
(b) the slope $\partial f/\partial x$ is small compared to unity, and
(c) the pressure p and the velocity component in the axial direction within the thread u_x are independent of the radial position σ.

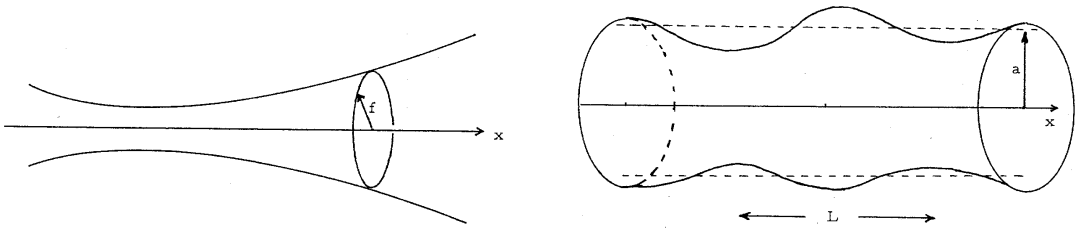

(a) (b)

Figure 1. (a) Illustration of a thinning axisymmetric thread immersed in an inviscid constant-pressure medium, evolving under the action of surface tension. (b) Capillary instability of an infinite thread with viscosity μ, immersed in an ambient fluid with viscosity $\lambda\mu$, subject to a periodic axisymmetric perturbation; a is the equivalent thread radius, and L is the wave length of the perturbation.

Following the physical derivation of Renardy [23], we perform a mass balance over a section of the thread contained between two cross-sections that are separated by an infinitesimal distance, and thus obtain the following evolution equation for f

$$\frac{\partial(\pi f^2)}{\partial t} + \frac{\partial(\pi f^2 u_x)}{\partial x} = 0. \tag{2.2}$$

Expanding the spatial derivative and simplifying, we find

$$\frac{\mathrm{D}f}{\mathrm{D}t} \equiv \frac{\partial f}{\partial t} + u_x \frac{\partial f}{\partial x} = -\frac{1}{2} f \frac{\partial u_x}{\partial x}, \tag{2.3}$$

where $\mathrm{D}/\mathrm{D}t = \partial/\partial t + u_x \partial/\partial x$.

An analogous momentum balance yields

$$\frac{\partial(\pi f^2 \rho u_x)}{\partial t} + \frac{\partial(\pi f^2 \rho u_x^2)}{\partial x} = \frac{\partial(\pi f^2 \sigma_{xx})}{\partial x} + \frac{\partial(2\pi f \gamma)}{\partial x}, \tag{2.4}$$

where ρ is the density of the thread fluid, γ is the surface tension, and σ_{xx} is the xx component of the stress tensor; for a Newtonian fluid

$$\sigma_{xx} = -p + 2\mu \frac{\partial u_x}{\partial x}, \tag{2.5}$$

where μ is the viscosity of the thread fluid. Equation (2.4) may be regarded as an evolution equation for the axial component of the velocity. To evaluate the pressure, we use the following approximate form of the interfacial dynamic boundary condition

$$\sigma_{\sigma\sigma} \equiv -p + 2\mu \frac{\partial u_\sigma}{\partial \sigma} \cong 2\kappa_m \gamma \cong -\frac{1}{f}\gamma, \tag{2.6}$$

where κ_m is the mean curvature of the interface. Near the thread axis, the continuity equation simplifies to

$$\frac{\partial u_x}{\partial x} + \frac{1}{\sigma}\frac{\partial(\sigma u_\sigma)}{\partial \sigma} \cong \frac{\partial u_x}{\partial x} + 2\frac{\partial u_\sigma}{\partial \sigma} \cong 0. \tag{2.7}$$

Combining Equations (2.6) and (2.7), we obtain

$$p = \frac{1}{f}\gamma - \mu\frac{\partial u_x}{\partial x}. \tag{2.8}$$

Substitution of expression (2.8) in Equation (2.5), and the result in Equation (2.4), gives

$$\rho\left(\frac{\partial(f^2u_x)}{\partial t} + \frac{\partial(f^2u_x^2)}{\partial x}\right) = 3\mu\frac{\partial}{\partial x}\left(f^2\frac{\partial u_x}{\partial x}\right) + \gamma\frac{\partial f}{\partial x}. \tag{2.9}$$

Finally, we use Equation (2.2) to simplify the left-hand side of (2.9), and arrive at the one-dimensional equation of motion

$$\rho\frac{\mathrm{D}u_x}{\mathrm{D}t} \equiv \rho\left(\frac{\partial u_x}{\partial t} + u_x\frac{\partial u_x}{\partial x}\right) = \frac{3\mu}{f^2}\frac{\partial}{\partial x}\left(f^2\frac{\partial u_x}{\partial x}\right) + \frac{\gamma}{f^2}\frac{\partial f}{\partial x}, \tag{2.10}$$

which is to be solved together with Equation (2.3) determining the evolution of the thread radius. Eggers [24] developed, and Brenner *et al.* [27] refined similarity solutions governing the local dynamics around the point of, and near the critical time for, breakup.

When inertial forces are negligible, the left-hand side and mid-side of Equation (2.10) may be set equal to zero. Integration of the resulting equation with respect to x yields

$$3\mu f^2\frac{\partial u_x}{\partial x} + \gamma f = q(t), \tag{2.11}$$

where $\pi q(t)$ is the axial force exerted on any thread cross-section. Combining Equations (2.11) and (2.3) we have the alternative set of equations

$$\frac{\mathrm{D}f}{\mathrm{D}t} = \frac{1}{6\mu}\left(\gamma - \frac{q(t)}{f}\right) \tag{2.12}$$

and

$$\frac{\partial u_x}{\partial x} = \frac{1}{3\mu}\left(-\frac{\gamma}{f} + \frac{q(t)}{f^2}\right). \tag{2.13}$$

Considering now a periodic interface with wave length L, we divide Equation (2.11) by f^2, integrate the resulting equation with respect to x over one period, and require a periodicity condition for the velocity to express $q(t)$ in terms of the instantaneous shape of the interface, as

$$q(t) = \gamma\int_b^{b+L}\frac{\mathrm{d}x}{f}\Big/\int_b^{b+L}\frac{\mathrm{d}x}{f^2}. \tag{2.14}$$

Equation (2.12) may be regarded as an evolution equation, determining the rate of change of the thickness of an infinitesimal thread section that is advected with the axial velocity. The coupling between the motions of the individual thread sections occurs solely through the integrals on the right-hand side of Equation (2.14). Renardy [23] labeled point particles along the thread axis with their axial position at a designated origin of time X regarded their instantaneous axial position as a function of X and time t, $x(X, t)$ and introduced the stretch

$s = \partial x/\partial X$. Kinematic considerations indicate that $\mathrm{D}s/\mathrm{D}t = s\partial u_x/\partial x$, and conservation of mass requires that $\mathrm{D}(sf^2)/\mathrm{D}t = 0$. Combining these equations with Equation (2.13), we obtain an evolution equation for $\mathrm{D}s/\mathrm{D}t$. On the basis of this equation, Renardy [23] showed that the thin-thread equations may possess singular solutions from smooth initial conditions.

Papageorgiou [25] searched for similarity solutions in the form

$$f(x,t) = b\tau^{\delta}\widehat{f}(\xi), \qquad u_x(x,t) = \frac{\gamma}{\mu}\tau^{\zeta}\widehat{u}_x(\xi), \tag{2.15}$$

where b is a characteristic length scale, a caret signifies a dimensionless variable, τ is a dimensionless time defined as

$$\tau \equiv \frac{\gamma}{\mu b}(t - t_c); \tag{2.16}$$

t_c is the critical time for thread breakup, ξ is a dimensionless similarity variable defined as

$$\xi \equiv \frac{x - x_c}{b\tau^{\beta}} \tag{2.17}$$

and x_c is the critical location where the breakup occurs. Substitution of expressions (2.15) in Equation (2.2) requires that $\zeta = \beta - 1$. Substituting expressions (2.15) in Equation (2.11), we obtain

$$6\gamma b\tau^{\delta-1}\left(-\delta\widehat{f} + (\beta\xi + \widehat{u}_x)\frac{\mathrm{d}\widehat{f}}{\mathrm{d}\xi}\right) = \gamma b - \frac{1}{\widehat{f}}\frac{q(t)}{\tau^{\delta}}. \tag{2.18}$$

The satisfaction of this relation requires a proper functional form for the force function $q(t)$ on the right-hand side.

Papageorgiou [25] considered a periodic thread with wave length L, and assumed that Equations (2.15) are valid within each period centered, for example, at the point hosting the pinch off. Integrating Equation (2.11) with respect to x over one period, and imposing the periodicity condition for the velocity, we find

$$q(t) = b\gamma c\tau^{\delta}, \tag{2.19}$$

where c is a dimensionless approximate constant defined as

$$c = \frac{\int_{x_c-L/2}^{x_c+L/2}\frac{\mathrm{d}x}{\widehat{f}(\xi)}}{\int_{x_c-L/2}^{x_c+L/2}\frac{\mathrm{d}x}{\widehat{f}^2(\xi)}} = \frac{\int_{(x_c-L/2)/(b\tau^{\beta})}^{(x_c+L/2)/(b\tau^{\beta})}\frac{\mathrm{d}\xi}{\widehat{f}(\xi)}}{\int_{(x_c-L/2)/(b\tau^{\beta})}^{(x_c+L/2)/(b\tau^{\beta})}\frac{\mathrm{d}\xi}{\widehat{f}^2(\xi)}}. \tag{2.20}$$

Substitution of Equation (2.19) in (2.18) requires $\delta = 1$ and produces an eigenvalue problem for β. Papageorgiou [25] convincingly argued that the main contributions to the integrals on the right-hand side of (2.20) are made from regions that are close to the point of break-up, and replaced the lower and upper limits of integration with $-\infty$ or $+\infty$. Equations (2.3) and (2.13) become

$$\frac{\mathrm{d}\log\widehat{f}}{\mathrm{d}\xi} = \frac{1 - \frac{1}{2}\frac{\mathrm{d}\widehat{u}_x}{\mathrm{d}\xi}}{\widehat{u}_x + \beta\xi} \tag{2.21}$$

and

$$\frac{\mathrm{d}\widehat{u}_x}{\mathrm{d}\xi} = \frac{1}{3}\frac{c-f}{\widehat{f}^2}. \tag{2.22}$$

To ensure that the right-hand side of (2.21) is finite, we require that the zeros ξ_0 of the numerator and denominator occur at the same location. Thus

$$1 - \frac{1}{2}\left(\frac{\mathrm{d}\widehat{u}_x}{\mathrm{d}\xi}\right)_{\xi=\xi_0} = 0 \tag{2.23}$$

and

$$\widehat{u}_x(\xi_0) + \beta\xi_0 = 0. \tag{2.24}$$

Equation (2.24), together with the condition that the velocity vanishes at $\xi = 0$, requires $\xi_0 = 0$. Equation (2.23) then provides us with the value $(\mathrm{d}\widehat{u}_x/\mathrm{d}\xi)_0 = 2$ which can be substituted in (2.22) to produce a quadratic equation relating the value of $\widehat{f}(\xi = 0)$ and the constant c

$$6\widehat{f}^2(\xi = 0) + \widehat{f}(\xi = 0) - c = 0. \tag{2.25}$$

A series expansion solution of the preceding equations provides us with a supplemental equation, as discussed by Papageorgiou [25], and the system has the solution

$$\widehat{f}(\xi = 0) = \frac{1}{12(1+\beta)}, \qquad c = \frac{1}{24}\frac{3+2\beta}{1+\beta)^2}. \tag{2.26}$$

The similarity solution predicts that near the time of breakup, the radius of the threads decreases linearly in time according to the scaling law

$$f(x_c, t) \cong \frac{\gamma}{12(1+\beta)\mu}(t_c - t). \tag{2.27}$$

Papageorgiou [25] solved the nonlinear eigenvalue problem and found $\beta = 0{\cdot}175$, to shown accuracy. Brenner *et al.* [27] discovered an inclusive family of solutions corresponding to other values of β, but the solution presented by Papageorgiou is the most stable one, and thus most likely to occur in practice. Furthermore, Papageorgiou [25] used a pseudo-spectral method to solve the model system of Equations (2.2) and (2.12) subject to a sinusoidal perturbation, and found excellent agreement with his similarity solution. Papageorgiou [21] recognized that the assumption that inertial effects are negligible is valid at all times only if β lies within the interval $(0{\cdot}5, 1)$. Since the computed value $\beta = 0{\cdot}175$ does not lie within this interval, the scaling (2.12) will eventually break down near the critical time for breakup.

The analysis of Papageorgiou assumes that, close to the critical time for breakup, $q(t)$ behaves linearly in time. Relaxing this restriction, we express $q(t)$ in the more general power-law form

$$q(t) = \gamma b q_0 \tau^{\chi}, \tag{2.28}$$

where q_0 is a dimensionless constant, and χ is a positive exponent. Equation (2.18) takes the form

$$6\tau^{\delta-1}\left(-\delta\,\widehat{f}+(\beta\xi+\widehat{u})\frac{\mathrm{d}\hat{f}}{\mathrm{d}\xi}\right)=1-q_0\frac{1}{\hat{f}}\tau^{\chi-\delta}. \tag{2.29}$$

When the exponents $\delta-1$ and $\chi-\delta$ are negative, the left-hand side and the second term on the right-hand side of (2.29) become singular at the critical time. Balancing the order of the singularities yields $\delta=(\chi+1)/2$. Renardy [26] discussed solutions for values of χ other than unity, but these values are associated with nonsmooth profiles that lie outside the scope of the present work.

3. Boundary-integral formulation

In this section, we describe a boundary-integral formulation that is suitable for simulating the evolution of a thread subject to a periodic perturbation, under conditions of Stokes flow. Consider a circular thread of a fluid with equivalent radius a and viscosity μ, immersed in an ambient fluid with viscosity $\lambda\mu$, subject to axisymmetric periodic disturbances with wave length L, as illustrated in Figure 1(b). To simulate the motion of the interface, we follow a well-established formalism, and derive the following Fredholm integral equation of the second kind for the interfacial velocity

$$\begin{aligned} u_\alpha(\boldsymbol{x}_0) \;=\; & \frac{1}{1+\lambda}\left(-\frac{1}{4\pi\mu}\int_C G_{\alpha\beta}(\boldsymbol{x}_0,\boldsymbol{x})\Delta f_\beta(\boldsymbol{x})\,\mathrm{d}l(\boldsymbol{x})\right. \\ & \left.+\frac{1-\lambda}{4\pi}\int_C{}^{PV} Q_{\alpha\beta\gamma}(\boldsymbol{x}_0,\boldsymbol{x})u_\beta(\boldsymbol{x})n_\gamma(\boldsymbol{x})\,\mathrm{d}l(\boldsymbol{x})\right), \end{aligned} \tag{3.1}$$

(Rallison and Acrivos [34], *e.g.* Pozrikidis [35, Chapter 5]). The point $\boldsymbol{x}_0$ lies in the interface, and the rest of the symbols are defined as follows: Greek subscripts run over the axial and radial polar cylindrical coordinates $\boldsymbol{x}$ or σ, C is one period of the contour of the interface in an azimuthal plane; l is the arc length along C; $\boldsymbol{n}$ is the unit vector normal to the interface pointing into the thread; PV denotes the principal value of the double-layer integral. The quantity $\Delta\boldsymbol{f}$ is a jump in the traction across the interface. For an interface with constant interfacial γ, $\Delta\boldsymbol{f}=2\kappa_m\gamma\boldsymbol{n}$ where κ_m is the interface mean curvature.

The kernels $\boldsymbol{G}$ and $\boldsymbol{Q}$ in Equation (3.1) are the periodic Green's functions of axisymmetric Stokes flow for the velocity and the stress, with wavelength matching that of the perturbation. As the radial position of the observation point σ_0 tends to infinity, all components of $G_{\alpha\beta}$ tend to vanish, except for G_{xx} that increases like $\ln(\sigma_0)$. In this limit, all components of $Q_{\alpha\beta\gamma}$ tend to decay like σ_0^{-2}, except for three components that decay like $8\pi\sigma/(RL\sigma_0)$. The computation of $\boldsymbol{G}$ and $\boldsymbol{Q}$ will be discussed in Subsection 3.2.

Starting with the singularly forced Stokes equation that defines the Green's function, and using the interpretation of the double-layer potential as a distribution of stresslets, we can show that the stress tensor $\boldsymbol{Q}$ satisfies the following integral identities

$$\int_C{}^{PV} Q_{\alpha x\gamma}(\boldsymbol{x}_0,\boldsymbol{x})n_\gamma(\boldsymbol{x})\,\mathrm{d}l(\boldsymbol{x})=4\pi\delta_{\alpha x} \tag{3.2a}$$

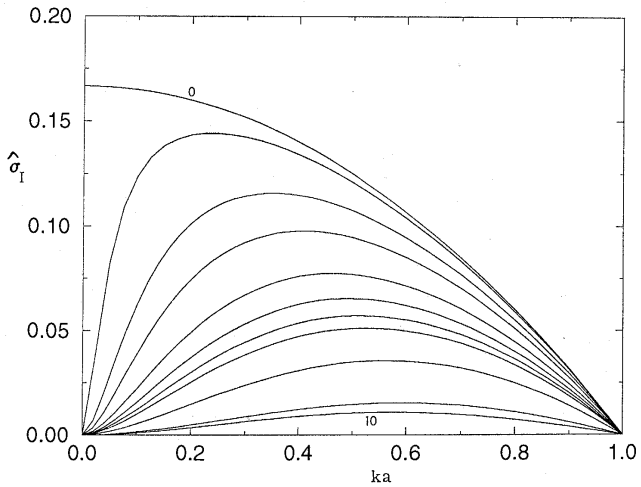

Figure 2. Instability of an infinite thread under conditions of Stokes flow; graphs of the reduced linear growth rate of axisymmetric perturbations, $\hat{\sigma}_I \equiv \mu a \sigma_I / \gamma$, in the regime of unstable wave numbers ka, for $\lambda = 0$, 0·01, 0·05, 0·1, 0·2, 0·3, 0·4, 0·5, 1·0, 5·0, 10·0.

and

$$\int_C^{PV} Q_{\beta\alpha\gamma}(\boldsymbol{x}, \boldsymbol{x}_0) \sigma n_\beta(\boldsymbol{x}) \, \mathrm{d}l(\boldsymbol{x}) = -4\pi \delta_{\alpha\gamma} \sigma_0. \tag{3.2b}$$

Identity (3.2a) suggests that, when $\lambda = 0$, Equation (3.1) has an infinite number of solutions that differ by an arbitrary constant vector oriented along the x axis. Physically, since the ambient fluid is inactive, the thread may translate as a rigid body along its axis with an arbitrary velocity. When the interface is symmetric with respect to a mid-point in each period, and the symmetry is exploited to half the integration domain C, the translational eigenfunction does not appear, and the solution of the integral equation is unique. More generally, we can remove the rigid-body-translation eigenfunction by replacing $\boldsymbol{u}$ in Equation (3.1) with a modified velocity $\boldsymbol{v}$, and also adding the following term to the right-hand side

$$-\delta_{\alpha x} \frac{1-\lambda}{1+\lambda} \frac{1}{S_D} \int_D v_x(\boldsymbol{x}) \, \mathrm{d}S(\boldsymbol{x}), \tag{3.3}$$

where D is one period of the interface. Once the solution for $\boldsymbol{v}$ has been found, the interfacial velocity can be recovered as follows. When $\lambda \neq 0$, we set

$$u_\alpha(\boldsymbol{x}_0) = v_\alpha(\boldsymbol{x}_0) + \delta_{\alpha x} \frac{1-\lambda}{2\lambda} \frac{1}{S_D} \int_D v_x(\boldsymbol{x}) \, \mathrm{d}S(\boldsymbol{x}). \tag{3.4}$$

When $\lambda = 0$, the fraction in the second term on the right-hand side of (3.4) is not defined, but this only means that the translational motion expressed by the second term can be arbitrary.

In the diametrically opposite limit where λ tends to infinity Equation (3.1) becomes

$$\begin{aligned} u_\alpha(x_0) \;=\; & -\frac{1}{4\pi(\lambda\mu)} \int_C G_{\alpha\beta}(\boldsymbol{x}_0, \boldsymbol{x}) \Delta f_\beta(\boldsymbol{x}) \, \mathrm{d}l(\boldsymbol{x}) \\ & -\frac{1}{4\pi} \int_C^{PV} Q_{\alpha\beta\gamma}(\boldsymbol{x}_0, \boldsymbol{x}) u_\beta(\boldsymbol{x}) n_\gamma(\boldsymbol{x}) \, \mathrm{d}l(\boldsymbol{x}). \end{aligned} \tag{3.5}$$

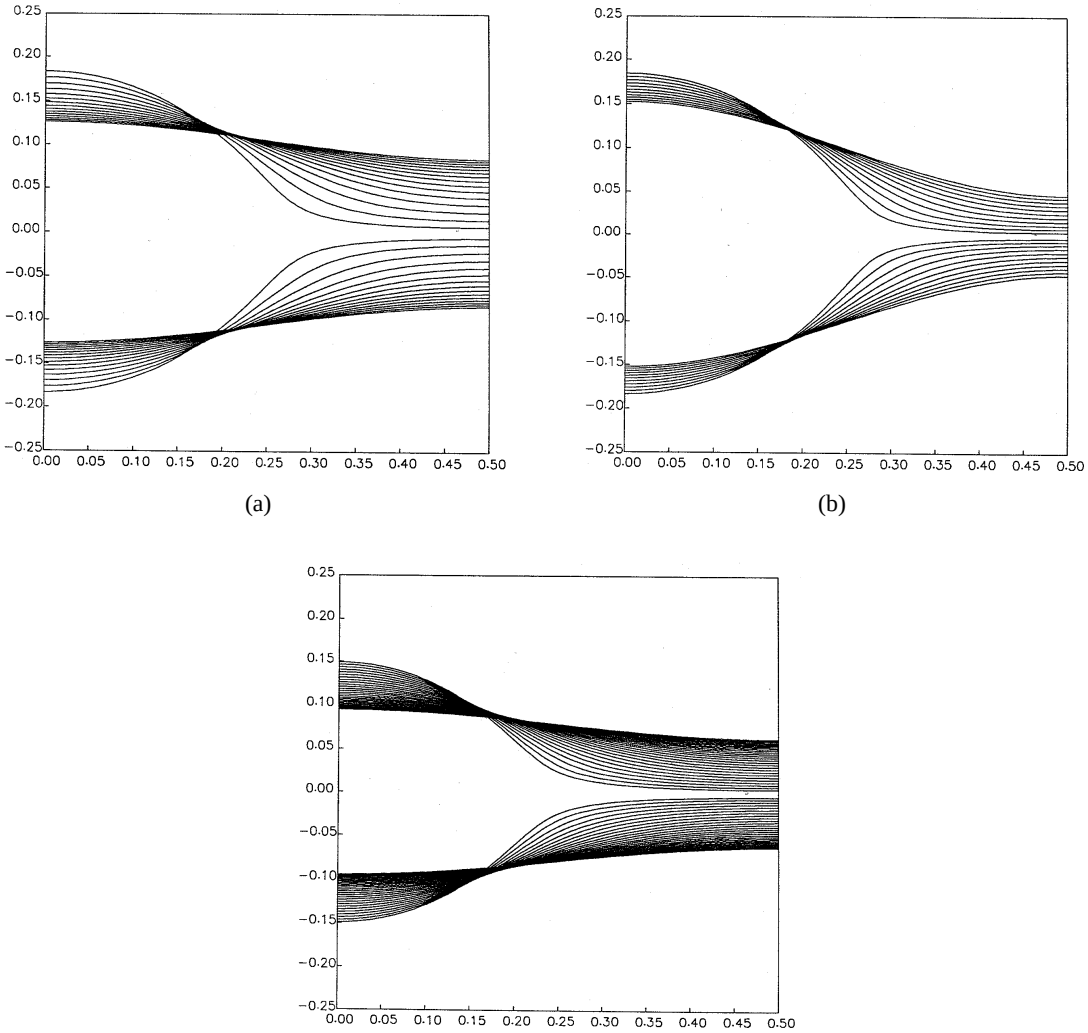

Figure 3. Sequences of evolving profiles over half the period of an axisymmetric perturbation, for viscosity ratio $\lambda = 0$; (a) $ka = \frac{2}{3}$, $a_1/a = 0{\cdot}2$, (b) $ka = \frac{2}{3}$, $a_1/a = 0{\cdot}5$, (c) $ka = 0{\cdot}5$, $a_1/a = 0{\cdot}20$.

The adjoint of the double-layer integral operator on the right-hand side of Equation (3.5) is

$$n_\gamma(\boldsymbol{x}_0) \int_C^{PV} Q_{\beta\alpha\gamma}(\boldsymbol{x}, \boldsymbol{x}_0) u_\beta(\boldsymbol{x}) \, \mathrm{d}l(\boldsymbol{x}). \tag{3.6}$$

Identity (3.2b) suggests that the adjoint of the integral Equation (3.5), and therefore the integral Equation (3.5) itself, has an infinite number of solutions that differ by a generally unknown eigenfunction. This eigenfunction can be removed by adding the following deflating term to the right-hand side of Equation (3.1)

$$n_\alpha(\boldsymbol{x}_0) \frac{1-\lambda}{1+\lambda} \int_D \boldsymbol{u}(\boldsymbol{x}) \cdot \boldsymbol{n}(\boldsymbol{x}) \sigma \, \mathrm{d}l(\boldsymbol{x}) \Big/ \int_D \sigma \, \mathrm{d}l(\boldsymbol{x}). \tag{3.7}$$

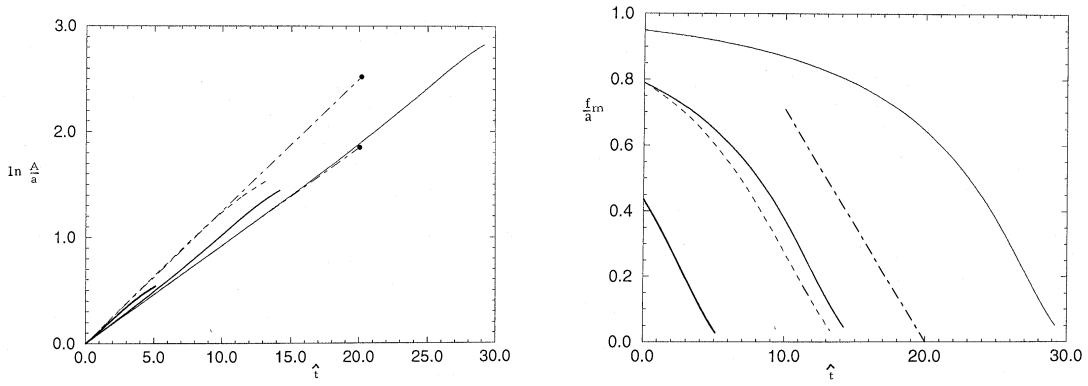

Figure 4. (a) Evolution of the amplitude of the disturbance A, defined as half the difference between the maximum and minimum thread radius, with respect to reduced time $\hat{t} \equiv \gamma t/\mu a$; the solid lines are for $ka = \frac{2}{3}$, with perturbation amplitudes $a_1/a = 0{\cdot}05$, $0{\cdot}2$, $0{\cdot}5$, corresponding to increasing line thickness; the dashed line corresponds to $ka = 0{\cdot}5$, and $a_1/a = 0{\cdot}20$; the long-short dashed lines ending at the bullets represent the predictions of the linear theory. (b) Corresponding evolution of the minimum thread radius, showing breakup at a finite time; the long-short dashed lines display the slope predicted by the similarity solution.

In the numerical method, when $\lambda \neq 0, \infty$, we solved the undeflated or deflated integral equation using either a direct method or the iterative method of successive substitutions implemented with Jacobi or Gauss-Siedel updates. For $\lambda = 0$, the deflated integral equation was solved by the direct method; discretization involving a boundary-element method with linear variation of the velocity and discontinuity in traction over the boundary elements produces a system of linear system of equations which is solved by the method of Gauss elimination.

To describe the motion of the interface, we trace one period of it in an azimuthal plane with a set of point particles, typically on the order of 100–250, approximate the contour of the interface with a collection of circular arcs, solve the integral equation for the velocity at the position of the point particles using a boundary-element method, and advance the position of the point particles using the second-order Runge-Kutta method. Points are added at regions of large curvature, or when two adjacent marker points have been separated by a large distance due to stretching. Numerical error causes the volume of the thread over a period to slight decrease during the simulations, but the change was less than $0{\cdot}5$ percent in all cases, and less than $0{\cdot}1$ percent in most cases. A complete simulation requires approximately 24 hours of CPU time on a SUN SPARCstation 20.

3.1. Computation of the Green's functions

The efficient and accurate computation of the periodic Green's functions $\boldsymbol{G}$ and $\boldsymbol{Q}$ is an important aspect of the numerical method. In the numerical procedure, we evaluated these functions by summing the nonperiodic free-space axisymmetric Green's functions, representing rings of point forces oriented in the axial or radial direction, indicated by the superscript Ring.

Expressions for the free space Green's functions in terms of complete elliptic integrals of the first and second kind are provided by Pozrikidis [34]. For example

$$G_{\alpha\beta}(x,\sigma,x_0,\sigma_0) = \sum_{k=-N}^{N} c_{|k|} G_{\alpha\beta}^{\text{Ring}}(x+kL,\sigma,x_0,\sigma_0), \tag{3.8}$$

where, for reasons that will soon become clear, we define $c_k = 1$ for $k = 1,\ldots,N-1$, and $c_N = \frac{1}{2}$; N is a specified truncation level, and L is the specified wave length. There is, however, one important exception: We note that G_{xx} decays like $4\pi\sigma/|x+kL-x_0|$, and prevent the divergence of its infinite sum by computing the modified sum

$$G_{xx}(x_0,\sigma_0,x,\sigma) = \sum_{k=-N}^{N} c_{|k|} \left(G_{xx}^{\text{Ring}}(x_0,\sigma_0,x+kL,\sigma) - \frac{4\pi\sigma}{|x+(k+\frac{1}{2})L|} \right). \tag{3.9}$$

Note that the last term within the sum is independent of the field-point coordinates (x_0,σ_0).

The summed terms in Equations (3.8) and (3.9) decay like $1/k^2$. To accelerate the rate of convergence, we use the error formula of the trapezoidal rule and find that the error E associated with the truncated sums (3.8) and (3.9) decays like $1/N$; that is

$$E(N) = \frac{\delta}{N}, \tag{3.10}$$

where δ is a constant (*e.g.* [36, p. 50]). This means that the sequence of errors corresponding to the sequence of truncation levels

$$N_0 = q, \qquad N_1 = pq, \qquad N_2 = p^2 q, \qquad N_3 = p^3 q, \ldots, \tag{3.11}$$

where p and q are two specified integers, satisfies the linear relation

$$E(N_k) = \frac{1}{p} E(N_{k-1}). \tag{3.12}$$

The convergence may then be accelerated by use of the method of Aitken extrapolation (*e.g.* [35, Chapter 1]. The numerical simulations reported in Section 4 were conducted in double precision with $q = 5$ or 10 and $p = 2$. The appropriate values for these two parameters must be found by numerical experimentation: Low values destroy the periodicity of the Green's function, and high values may cause numerical underflow due to the subtraction of numbers with comparable magnitudes in carrying out the Aitken extrapolation.

4. Results and discussion

In Figure 2, we present graphs of the reduced linear growth rate $\widehat{\sigma}_I \equiv \gamma\sigma_I/\mu a$ of axisymmetric perturbations, plotted against the reduced wave number ka, for several values of the viscosity ratio λ, generated from analytical formulas provided by Tomotika [14] in terms of Bessel functions; a is the equivalent thread radius, and σ_I is the imaginary part of the complex growth rate. As λ tends to zero, we observe a singular behavior: The graphs become steep near the origin of the wave number axis, and the wave number corresponding to maximum growth

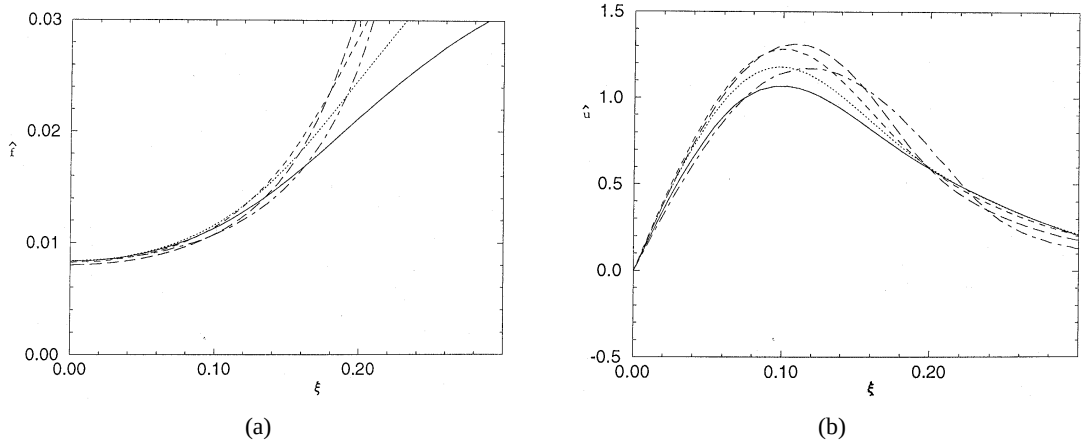

(a) (b)

Figure 5. Comparison of the numerical results with the similarity solution: (a) scaled thread radius, and (b) scaled axial velocity, defined in equations (4.1), for $ka = \frac{2}{3}$, $a_1/a = 0{\cdot}2$. The solid, dotted, dashed, long dashed, and dot-dashed lines correspond, respectively to times $t\gamma/\mu a = 10, 11, 12, 13, 14$.

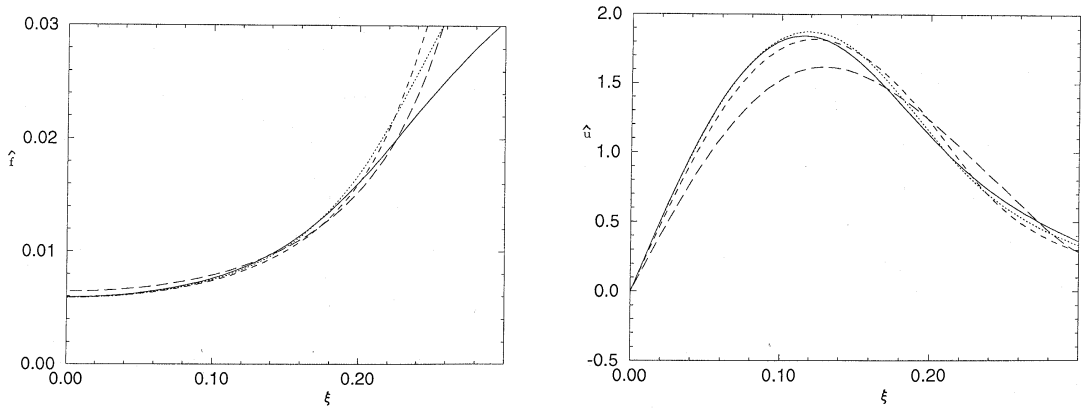

(a) (b)

Figure 6. Same as Figure 5, but for $ka = 0{\cdot}5$, $a_1/a = 0{\cdot}2$. The solid, dotted, dashed, and long dashed correspond, respectively to times $t\gamma/\mu a = 10, 11, 12, 13$.

rate is shifted toward zero indicating that the longer a wave, the faster it grows. Increasing the viscosity of the ambient fluid causes a significant reduction in the growth rate of the perturbations. In the limit as λ tends to infinity, corresponding to an inviscid thread suspended in a viscous fluid, rescaling of the time with respect to the viscosity of the ambient fluid is necessary.

In Figure 3(a–c), we present sequences of evolving profiles over half a period of a sinusoidal perturbation with initial amplitude a_1, for $\lambda = 0$ and for the conditions described in the figure caption, computed by the boundary-integral method. The profiles correspond to evenly spaced time intervals between the origin of time and the last time shown in Figure 4. In all cases, the reduced wave number ka is less than unity: The instability amplifies, as

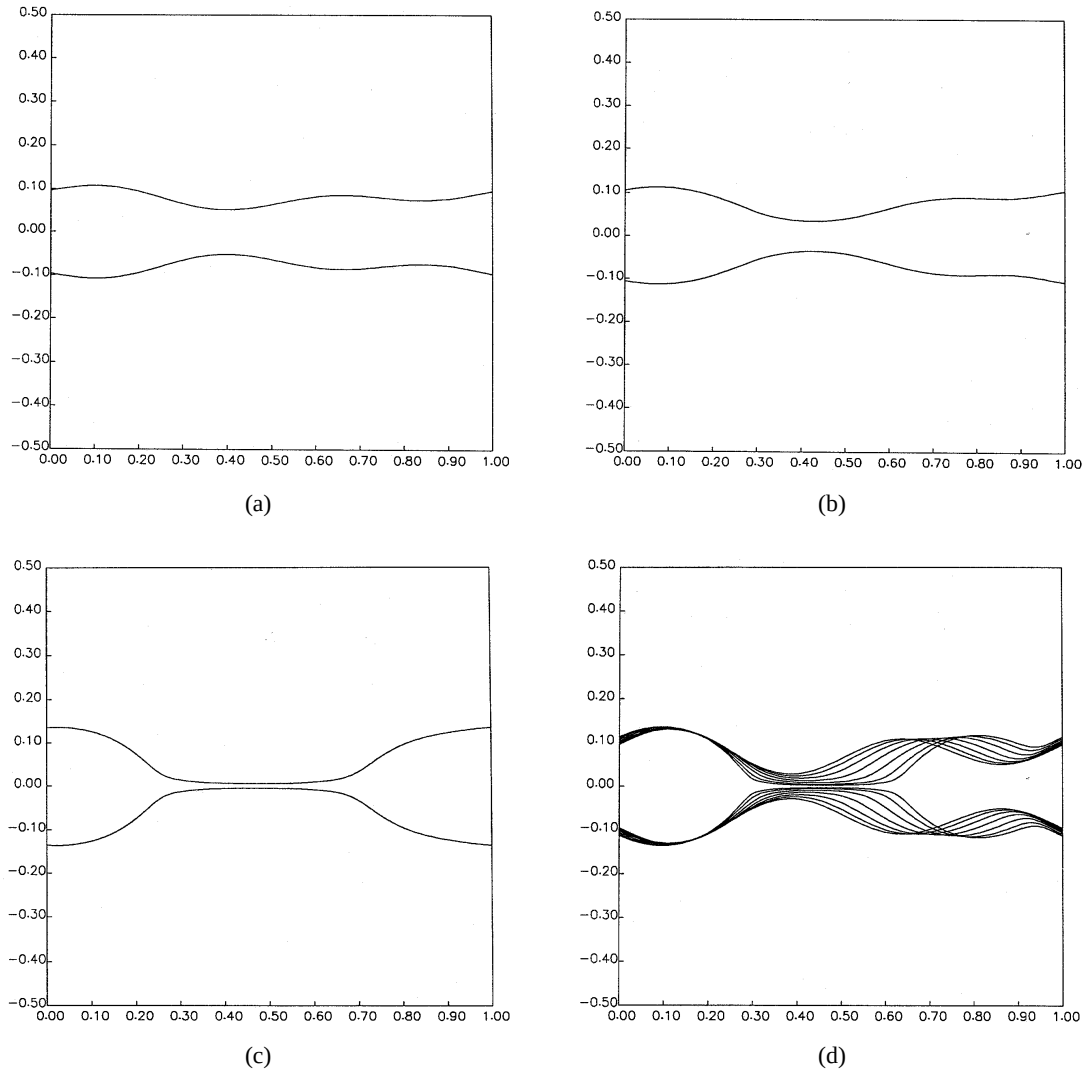

Figure 7. (a–c) Stages in the evolutioin of a thread for a bi-chromatic perturbation described by Equation (4.3) with $ka_0 = 0{\cdot}5$, $a_1/a_0 = 0{\cdot}20$ and $a_2/a_0 = 0{\cdot}20$, at times $\widehat{t} \equiv \gamma t/\mu a_0 = 0, 3{\cdot}5, 7{\cdot}5$; (d) Stages in the evolution of a thread for a bi-chromatic perturbation described by Equation (4.3) with $ka_0 = 0{\cdot}5$, $a_1/a_0 = 0{\cdot}20$ and $a_2/a_0 = 0{\cdot}50$, at times $\widehat{t} \equiv \gamma t/\mu a_0 = 0, 0{\cdot}5, 1{\cdot}0, 2{\cdot}0, 2{\cdot}5, 2{\cdot}848$.

predicted by linear theory, and the thread tends to break up at the mid-point of each wave length corresponding to the trough of the sinusoidal perturbation. The long time shape of the thread consists of a periodic sequence of drops connected by thinning links.

In Figure 4(a), we plot the amplitude of a disturbance A, defined as half the difference between the maximum and minimum thread radius, against time, on a linear-logarithmic scale, for several types of perturbation. The agreement between the numerical results, represented by the solid lines, and the predictions of the linear theory, represented by the long-short dashed lines marked by the bullets, is excellent even when the amplitude of the disturbance is not

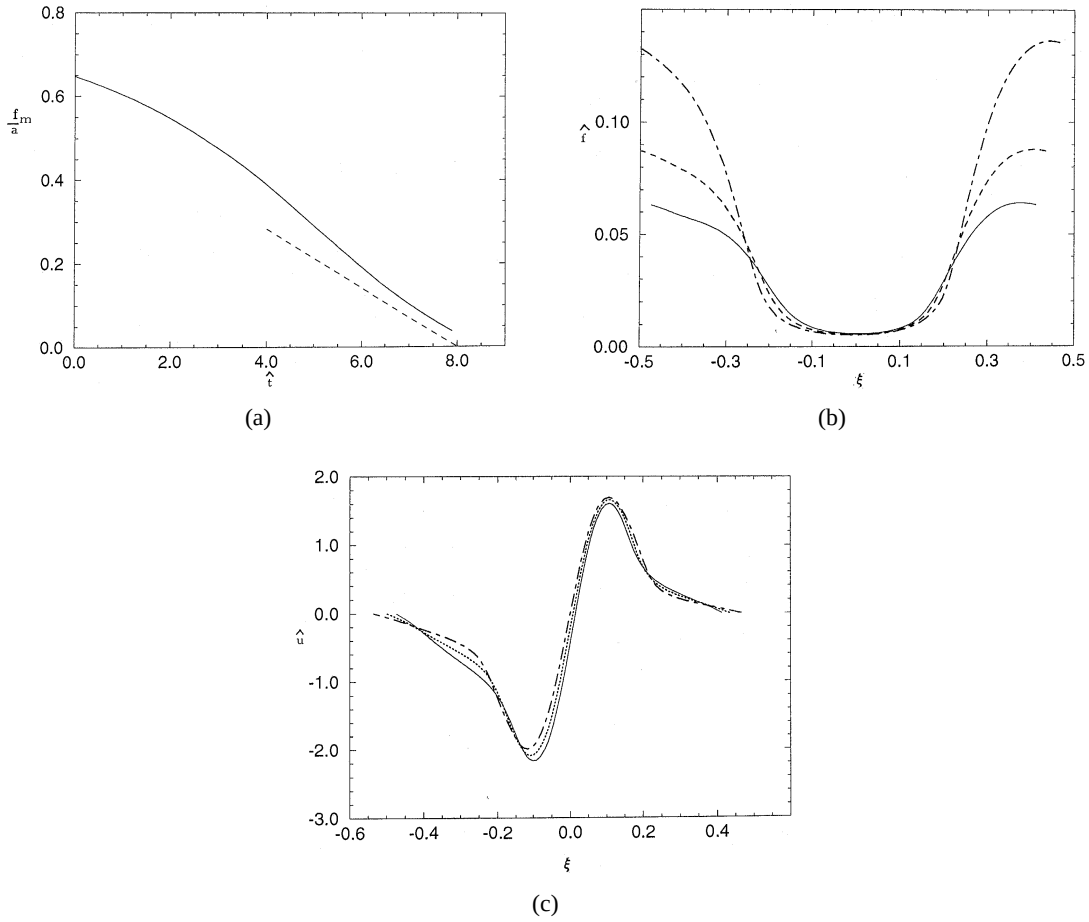

Figure 8. Details of the motion shown in Figure 7(a–c): (a) evolution of the minimum thread radius, showing breakup at a finite time; (b) scaled thread radius, and (c) scaled axial velocity, defined in Equations (4.1) plotted against the similarity variable defined in Equation (4.2), for $\widehat{t} \equiv \gamma t/\mu a_0 = 6{\cdot}5,\ 7{\cdot}0,\ 7{\cdot}5$.

infinitesimal. In Figure 4(b), we plot the minimum thread radius f_m against time on a linear-linear scale. In all cases, the numerical results clearly indicate that the minimum radius tends to vanish at a finite critical time t_c whose precise value depends on the wave length and amplitude of the perturbation. Near the critical time, all curves tend to become linear with a common slope that is in excellent agreement with that predicted by Papageorgiou's similarity solution, described by Equation (2.27) with $\beta = 0{\cdot}175$, and represented by the straight dashed line in Figure 4(b).

As the critical time approaches, the intensity of the axisymmetric stagnation-point flow prevailing near the point of breakup increases at an algebraic rate, in agreement with the similarity solution. To demonstrate the agreement in quantitative terms, in Figure 5 and 6 we plot profiles of the scaled functions

$$\widehat{f} \equiv \frac{f(\widehat{x}, t)}{L\tau}, \qquad \widehat{u} \equiv \frac{\mu}{\gamma \tau^{1-\beta}} u_x^I(\widehat{x}, t), \tag{4.1}$$

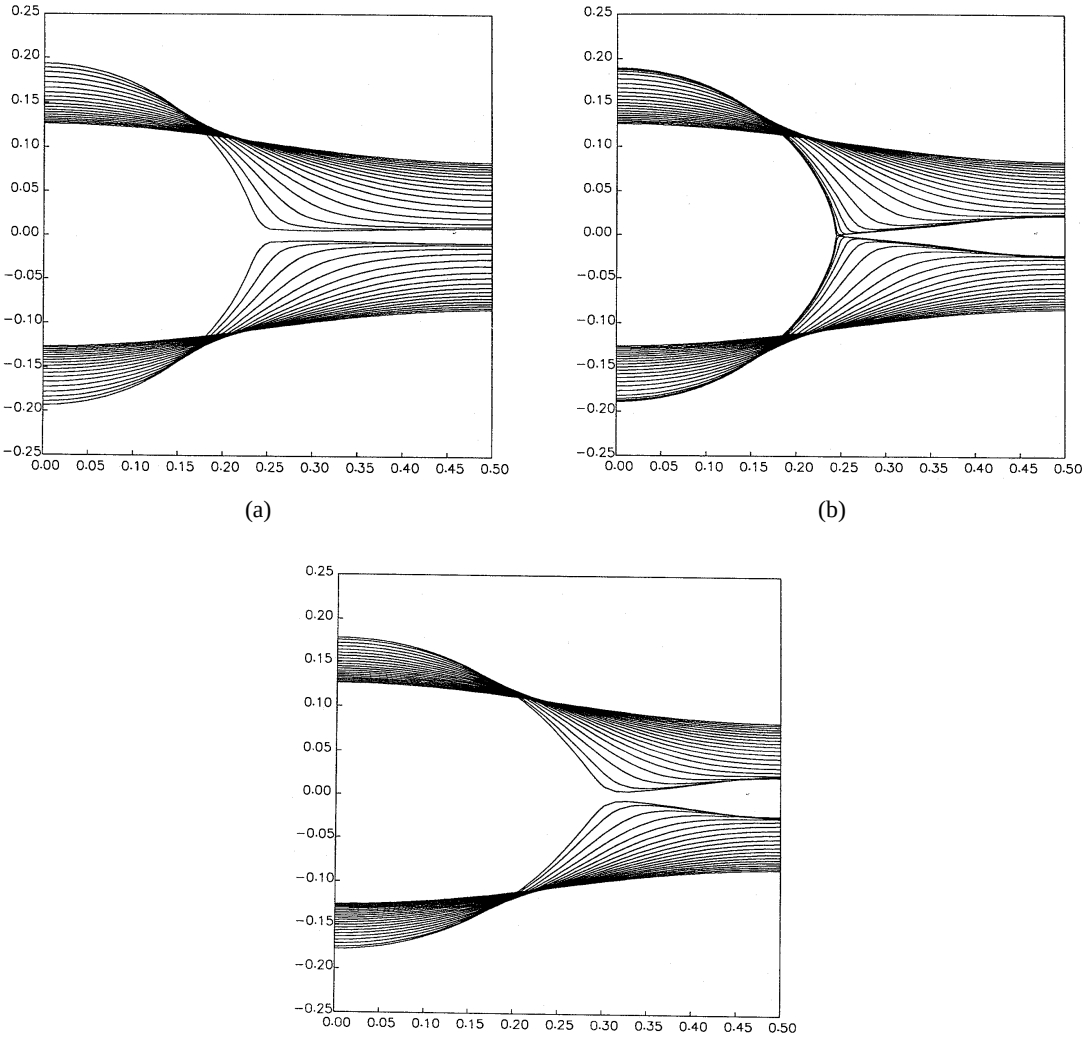

Figure 9. Sequences of evolving profiles over half the period of an axisymmetric perturbation, for $ka = \frac{2}{3}$, $a_1/a = 0{\cdot}2$, and viscosity ratio (a) $\lambda = 0{\cdot}05$, (b) 1·0, (c) 5·0.

where L is the wave length of the perturbation, and $u_x^I(x,t)$ is the axial component of the velocity along the interface, against the similarity variable

$$\xi \equiv \frac{x - x_c}{L} \frac{1}{\tau^\beta} \tag{4.2}$$

for $\beta = 0{\cdot}175$. Figure 5 corresponds to a perturbation with $ka = \frac{2}{3}$, $a_1/a = 0{\cdot}20$, and Figure 6 corresponds to a perturbation with $ka = 0{\cdot}5$, $a_1/a = 0{\cdot}20$; both are unstable according to linear theory. The critical times, $t_c = 14{\cdot}75\mu a/\gamma$ and $13{\cdot}65\mu a/\gamma$, were found by extrapolating the data shown in Figure 4(b). The times corresponding to the various profiles are given in the figure captions. According to the similarity solution, the scaled functions

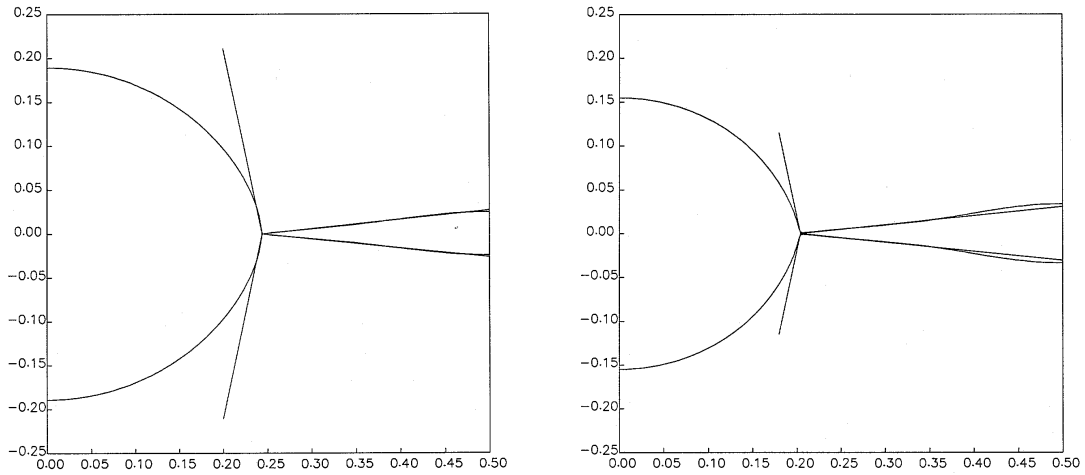

Figure 10. The shape of the interface close to the time of breakup for $\lambda = 1$ and (a) $ka = 0{\cdot}5$ (b) $\frac{2}{3}$, plotted along with the cone angles deduced from the numerical results of Lister and Stone.

(4.1) possess a universal functional form subject to linear scaling of the similarity variable ξ by a factor that is determined by the initial condition. The results shown in Figures 5 and 6 are in good agreement with the theoretical predictions over a substantial portion of the thread around the point of breakup, up to the point where the thin-thread approximation ceases to be valid. Furthermore, the shapes of the scaled functions shown in the graphs are similar in form to those graphed by Papageorgiou [25]. The similarity solution predicts that $f(x = x_c, t)/L\tau = 1/(12(1+\beta)) = 0{\cdot}0709$ irrespective of the initial conditions, and this value is consistent with the numerical results presented in Figures 5(a) and 6(a).

Papageorgiou [25] carried out numerical solutions of the thin-thread equations for $ka_0 = 0{\cdot}5$ and $a_1/a_m = 0{\cdot}20$, where a_0 is the mean thread radius, related to the equivalent radius a by $a_0^2 = a^2 - 0{\cdot}5a_1^2$. These initial conditions are almost, but not precisely, identical to those used in the boundary-integral simulations presented in Figure 3(c) and 6. The evolution of the thread predicted by the thin-thread model is qualitatively similar to that generated by the boundary-integral method. The critical time for breakup predicted by the thin-thread model, $t_c = 13{\cdot}281\mu a/\gamma$, is surprisingly close to the value $13{\cdot}65\mu a/\gamma$ predicted by the present simulations. This good agreement suggests that further conclusions drawn by Papageorgiou on the basis of his numerical investigations are also likely to be valid in the more inclusive context of Stokes flow.

The numerical results presented thus far correspond to monochromatic perturbations: The interface is symmetric with respect to the trough of the initial sinusoid, and remains so throughout the evolution. The similarity solution also predicts locally symmetric shapes, but it is not clear that these will arise from nonsymmetric initial conditions. To solve this issue, we simulated the evolution of the thread subject to disturbances comprised of a fundamental wave and its first harmonic. At the initial instant, the trace of the interface in an azimuthal plane is described by the equation

$$s = a_0 + a_1\cos(kx) + a_2\sin(2kx), \tag{4.3}$$

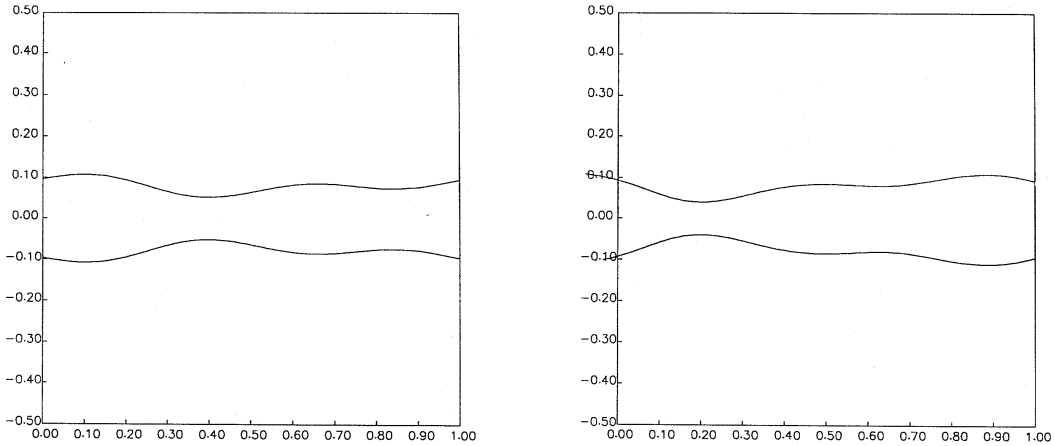

(a) (b)

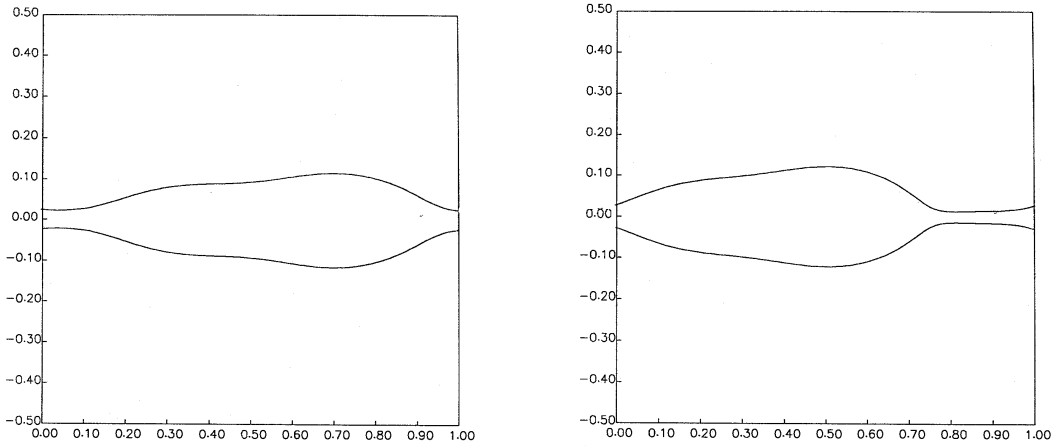

(c) (d)

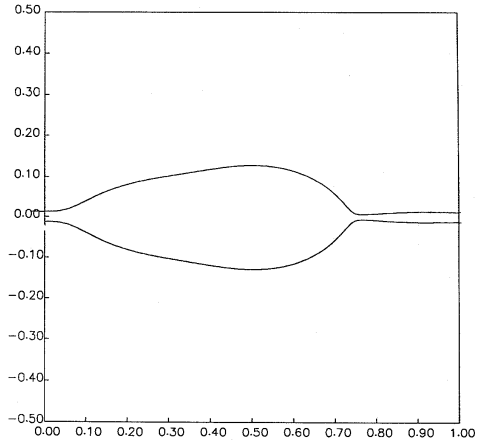

(e)

Figure 11. (a–e) Stages in the evolution of a thread for a bi-chromatic perturbation described by Equation (4.3) with $ka_0 = 0{\cdot}5$, $a_1/a_0 = 0{\cdot}20$ and $a_2/a_0 = 0{\cdot}20$, at times $\widehat{t} \equiv \gamma t/\mu a_0 = 0, 5, 20, 25, 29$.

where k is the wave number of the fundamental wave. Figure 7(a–c) shows a sequence of profiles for $ka_0 = 0{\cdot}5$, $a_1/a_0 = 0{\cdot}20$ and $a_2/a_0 = 0{\cdot}20$, and Figure 7(d) shows a sequence of profiles for $ka_0 = 0{\cdot}5$, $a_1/a_0 = 0{\cdot}20$ and $a_2/a_0 = 0{\cdot}50$, in both cases over a full wave length of the fundamental. In both cases, the fundamental wave is unstable, whereas the harmonic wave is neutrally stable according to linear theory. In both cases, the unstable wave dominates the evolution, the thread breaks up at a finite time, and the local structure of the flow and shape of the interface are symmetric about the point of breakup near the critical time.

To demonstrate these behaviors more explicitly, in Figure 8(a) we plot the evolution of the minimum thread radius against time, for the conditions corresponding to Figure 7(a–c). Near the critical time for breakup, $t_c = 8{\cdot}5\mu a_0/\gamma$ estimated by extrapolation, we observe a linear behavior with a slope that is in good agreement with that predicted by the similarity solution, represented by the dashed line. In Figure 8(b,c) we plot the scaled interface profile and axial velocity defined in Equations (4.1), against the similarity variable defined in Equation (4.2), at dimensionless times $\widehat{t} \equiv \gamma t/\mu a_0 = 6{\cdot}5, 7{\cdot}0, 7{\cdot}5$, for $x_c/L = 0{\cdot}465$ estimated by extrapolation, and obtain locally symmetric and nearly universal shapes. These results provide us with strong numerical evidence that the similarity solution is relevant to a broad range of symmetric or unsymmetric initial conditions.

Papageorgiou [21] noted that inertial effects become important when the axial acceleration of the fluid within the thread has reached sufficiently high levels. When this has occurred, the similarity solution ceases to be valid, and a different kind of thinning, possibly described by Egger's [24] similarity solution, is expected to prevail. Such a transition was noted in the experiments of Kowalewski [37]. Confirming it, however, in the context of Navier-Stokes flow must await the development of sophisticated numerical methods.

Next, we consider the effect of the viscosity of the ambient fluid. In Figure 9(a–c), we display sequences of evolving profiles for a sinusoidal perturbation with $ka = \frac{2}{3}$, and $a_1/a = 0{\cdot}20$, corresponding to viscosity ratio $\lambda = 0{\cdot}05, 1{\cdot}0, 5{\cdot}0$. It is clear that the viscosity of the ambient fluid plays an important role in determining the dynamics of thinning, the location of the point of breakup, and the geometry of the interfacial shape near the point of breakup. When $\lambda = 0{\cdot}05$, the links connecting successive drops are nearly cylindrical, and breakup is expected to occur away from the mid-point; numerical difficulties prevented us from continuing the simulation beyond the last stage shown in the figure. The shifting of the breakup point is clearly evident in Figure 9(b) corresponding $\lambda = 1$. In this case, the boundary-integral equation reduces to an integral representation, and this simplification has allowed us to carry out the simulation virtually up to the point of interface touching. Similar shapes were presented by Newhouse and Pozrikidis [17] and recently by Lister and Stone [33].

Lister and Stone [33] simulated the relaxation of an extended axisymmetric drop whose viscosity is equal to that of the ambient fluid, and found that breakup occurs at a finite time, in agreement with the results of our simulations for $\lambda = 1$. The shape of the interface near the point of pinching is similar to that shown in Figure 9(b), consisting of a double cone with aperture angles equal to $5{\cdot}9^\circ$ and $78{\cdot}2^\circ$. In Figure 10(a,b), we plot the shape of the interface very close to the time of breakup for $\lambda = 1$ and $ka = 0{\cdot}5$ and $\frac{2}{3}$, along with the cones angles deduced by Lister and Stone, and find excellent agreement, thus confirming the independence of the process of breakup on the initial conditions. Lister and Stone used high resolution by deploying up to $4,000$ marker points over the interface, to describe the shape of the interface near the point of pinching. Unfortunately, high computational cost due to the expensive evaluation of the periodic Green's function has prevented us from duplicating their analysis.

To investigate further whether nonsymmetric initial conditions develop in different ways, we simulated to motion of a thread for $\lambda = 1$, with the initial shape described by Equation (4.3), for $ka_0 = 0{\cdot}5$, $a_1/a_0 = 0{\cdot}20$ and $a_2/a_0 = 0{\cdot}20$. In Figure 11(a–e), we present typical stages in the evolution up to the point where breakup is about to occur on one side. The partial similarity between the shapes at the two ends of the developing unsymmetric drops with the shapes shown in Figure 9(b) suggest that the evolution near the point of breakup might be universal, but the numerical evidence is not strong enough to be conclusive.

A simplified set of equations describing the evolution of a thinning thread in the presence of a viscous ambient fluid has not been developed. In setting up such a theory, one may approximate the flow within the thread with a uniaxial axisymmetric extensional flow added to a parabolic flow, and represent the outer flow in terms of either the velocity or the shear stress exerted on either side of the interface using, for example, the boundary-integral method. The shear stress corresponding to the uniaxial axisymmetric extensional flow vanishes on either side of the interface independent of the viscosities of the fluids, but the normal stress undergoes a jump by an amount that is proportional to the viscosity difference and the local rate of extension (Tomotika [38], Mikami, Cox and Mason [39]). The subtlety of computing the outer extensional flow challenges the search for similarity solution describing universal behaviors.

Acknowledgments

This research was supported by the *National Science Foundation.* Acknowledgment is made to the Donors of the *Petroleum Research Fund*, administered by the *American Chemical Society*, for partial support.

References

1. M. Tjahjadi and J. M. Ottino, Stretching and breakup of droplets in chaotic flows. *J. Fluid Mech.* 232 (1991) 191–219.
2. A. H. P. Skelland and P. G. Walker, The effects of surface active agents on jet breakup in liquid-liquid systems. *Can. J. Chem. Eng.* 67 (1989) 762–770.
3. A. H. P. Skelland and E. A. Slaymaker, Effects of surface-active agents on drop size in liquid-liquid systems. *Ind. Eng. Chem. Res.* 29 (1990) 494–499.
4. D. B. Bogy, Drop formation in a circular liquid jet. *Ann. Rev. Fluid Mech.* 11 (1979) 207–228.
5. R. R. Allen, J. D. Meyer, and W. R. Knight, Thermodynamics and hydrodynamics of thermal ink jets. *Hewlett–Packard Journal*, May issue (1985) 221–227.
6. D. M. Henderson, W. G. Pritchard, and L. B. Smolka, On the pinch-off of a pendant drop of viscous fluid. *Phys. Fluids* 9 (1997) 3188–3200.
7. C. V. Boys *Soap Bubbles*. New York: Dover (1959) 192 pp.
8. J. Eggers, Nonlinear dynamics and breakup of free-surface flows. *Rev. Modern Phys.* 69 (1997) 865–930.
9. S. P. Lin and R. D. Reitz, Drop and spray formation from a liquid jet. *Annu. Rev. Fluid Mech.* 30 (1998) 85–105.
10. J. Plateau *Statique Experimentale et Theoretique des Liquides Soumis aux Seules Forces Moleculaires*. Paris: Gautier-Villars (1873) 495 pp.
11. L. Rayleigh, On the instability of jets. *Proc. London Math. Soc.* 10 (1878) 4–13.
12. L. Rayleigh, On the stability of a cylinder of viscous liquid under capillary force *Phil. Mag.* 34 (1892) 145.
13. Z. Z. Weber, Zum Zerfall eines Flüssigkeitsstrahles, *Z. Math. Mech.* 11 (1931) 136–154.
14. S. Tomotika, On the instability of a cylindrical thread of a viscous liquid surrounded by another viscous fluid. *Proc. Roy. Soc.* A 150 (1935) 322–337.
15. S. L. Goren, The instability of an annular layer thread of fluid. *J. Fluid Mech*. 13 (1962) 309–319.

16. S. L. Goren, The shape of a thread of liquid undergoing breakup. *J. Colloid Sci*. 19 (1964) 81–86.
17. L. A. Newhouse and C. Pozrikidis, The capillary instability of annular layers and liquid threads. *J. Fluid Mech*. 242 (1992) 193–209.
18. F. D.Rumscheidt and S. G. Mason, Break-up of stationary liquid threads. *J. Colloid Sci*. 17 (1962) 260–269.
19. P. H. M. Elemans, J. M. H. Janssen, and, H. E. H. Meijer, The measurement of interfacial tension in polymer/polymer systems: The breaking thread method. *J. Rheol*. 34 (1990) 1311–1325.
20. J. M. H. Janssen, *Dynamics of liquid-liquid mixing*. Doctoral Dissertation, Technische Universiteit Eindhoven, The Netherlands (1993) 117 pp.
21. D. T. Papageorgiou, Description of jet breakup. In: Y. Y. Renardy, A. C. Coward, D. T. Papageorgiou and S. M. Sun (eds), *Adv. Multi-Fluid Flows*. Philadelphia: SIAM (1996).
22. H. C. Lee, Drop formation in a liquid jet. *IBM J. Res. Dev.* 18 (1974) 364–369.
23. M. Renardy, Some comments on the surface-tension driven break-up (or the lack of it) of viscoelastic jets. *J. Non-Newt. Fluid Mech*. 51 (1994) 97–107.
24. J. Eggers, Universal pinching of 3D axisymmetric free-surface flow. *Phys. Rev. Letters* 71 (1993) 3458–3460.
25. D. T. Papageorgiou, On the breakup of viscous liquid threads. *Phys. Fluids* 7 (1995) 1529–1544.
26. M. Renardy, A numerical study of the asymptotic evolution and breakup of Newtonian and viscoelastic jets. *J. Non-Newt. Fluid Mech.* 51 (1995) 97–107.
27. M. P. Brenner, J. R. Lister, and H. A. Stone, Pinching threads, singularities and the number 0·0304 . . . *Phys. Fluids* 8 (1996) 2827–2836.
28. D. W. Bousfield, R. Keunings, G. Marrucci and M. M. Denn, Nonlinear analysis of the surface tension driven breakup of viscoelastic filaments. *J. Non-Newt. Fluid Mech.* 21 (1986) 79–97.
29. N. N. Mansour and T. S. Lundgren, Satellite formation in capillary jet breakup. *Phys. Fluids* A 2 (1990) 1141–1144.
30. M. H. Tjahjadi, H. A. Stone, and J. M. Ottino, Satellite and subsatellite formation in capillary breakup. *J. Fluid Mech.* 243 (1992) 297–317.
31. J. R. Richards, A. M. Lenhoff, and A. N. Beris, Dynamic breakup of liquid-liquid jets. *Phys. Fluids* 6 (1994) 2640–2655.
32. J. R. Richards, A. N. Beris, and A. M. Lenhoff, Drop formation in liquid-liquid systems before and after jetting. *Phys. Fluids* 7 (1995) 2617–2630.
33. J. R. Lister, and H. A. Stone, Capillary breakup of a viscous thread surrounded by another viscous fluid. *Phys. Fluids* 10 (1998) 2758–2764.
34. J. M. Rallison and A. Acrivos, A numerical study of the deformation and burst of a viscous drop in an extensional flow. *J. Fluid Mech.* 89 (1978) 191–200.
35. C. Pozrikidis, *Boundary Integral and Singularity Methods for Linearized Viscous Flow*. Cambridge: Cambridge University Press (1992) 259 pp.
36. C. Pozrikidis, *Numerical Computation in Science and Engineering*. Oxford: Oxford University Press (1998) 627 pp.
37. T. A. Kowalewski, On the separation of droplets from a liquid jet. *Fluid Dyn. Res.* 17 (1996) 121–145.
38. S. Tomotika, Breakup of a drop of viscous liquid immersed in another viscous fluid which is extending at a uniform rate. *Proc. Roy. Soc.* A 153 (1936) 302–318.
39. T. Mikami, R. G. Cox, and S. G. Mason, Breakup of extending liquid threads. *Int. J. Multiphase Flow* 2 (1975) 113–138.